

A Universal Design Strategy Based on NiPS₃ Nanosheets towards Efficient Photothermal Conversion and Solar Desalination

Honglei Wang, Yifan Bo, Malte Klingenhof, Jiali Peng, Dong Wang,* Bing Wu, Jörg Pezoldt, Pengfei Cheng,* Andrea Knauer, Weibo Hua, Hongguang Wang,* Peter A. van Aken, Zdenek Sofer, Peter Strasser, Dirk M. Guldi,* and Peter Schaaf


2D nanomaterials are proposed as promising photothermal materials for interfacial photothermal water evaporation. However, low evaporation efficiency, the use of hazardous hydrofluoric solution, and poor stability severely limit their practical applications. Here, a mixed solvent exfoliation surface deposition (MSESD) strategy for the preparation of NiPS₃ nanosheets and NiPS₃/polyvinyl alcohol (PVA) converter is successfully developed. The converter is obtained by drop-casting the NiPS₃/PVA nanosheets onto a sponge. The PVA is mainly deposited on the edge of NiPS₃ nanosheets, which not only improves the stability of NiPS₃ nanosheets, but also adheres to the sponge to prepare a 3D photothermal converter, which shows an evaporation rate of 1.48 kg m⁻² h⁻¹ and the average photothermal conversion efficiency (PTCE) of 93.5% under a light intensity of 1 kW m⁻². The photothermal conversion mechanism reveals that the energy of absorbed photons in NiPS₃ nanosheets can be effectively converted into heat through non-radiative photon transitions as well as multiple optical interactions. To the best of the knowledge, this is the first report on the application of 2D metal-phosphorus-chalcogen (MPCh_x) for solar desalination, which provides new insights and guidance for the development of high-performance 2D photothermal materials.

1. Introduction

Global population growth, rapid industrialization, and environmental pollution have exacerbated the energy crisis and freshwater scarcity.^[1] Therefore, it is urgent to develop low-cost and environmentally friendly photothermal conversion technologies to efficiently collect solar energy for solar desalination.^[2] 2D materials have attracted increasing attention from researchers due to their unique physical and chemical properties, such as large specific surface area and tunable band gap.^[3] However, although 2D materials have achieved great success in photothermal conversion and solar desalination, there are still various obstacles. The exfoliation efficiency of 2D transition-metal dichalcogenides (TMDs) is low,^[4] the preparation of transition metal carbides and nitrides (MXenes) requires the use of hazardous hydrofluoric solution,^[5] and black phosphorus (BP) is prone to oxidation and decomposition under air and humid

H. Wang, D. Wang, P. Cheng, P. Schaaf
Chair Materials for Electrical Engineering and Electronics
Institute of Materials Science and Engineering and Institute of Micro and Nanotechnologies MacroNano
TU Ilmenau
Gustav-Kirchhoff-Str. 5, 98693 Ilmenau, Germany
E-mail: dong.wang@tu-ilmenau.de; pengfei.cheng@tu-ilmenau.de

Y. Bo, D. M. Guldi
Department of Chemistry and Pharmacy
Interdisciplinary Center for Molecular Materials
Friedrich-Alexander-Universität (FAU) Erlangen-Nürnberg
Egerlandstraße 3, 91058 Erlangen, Germany
E-mail: dirk.guldi@fau.de

 The ORCID identification number(s) for the author(s) of this article can be found under <https://doi.org/10.1002/adfm.202310942>

© 2023 The Authors. Advanced Functional Materials published by Wiley-VCH GmbH. This is an open access article under the terms of the Creative Commons Attribution License, which permits use, distribution and reproduction in any medium, provided the original work is properly cited.

DOI: 10.1002/adfm.202310942

M. Klingenhof, P. Strasser
The Electrochemical Energy, Catalysis
and Materials Science Laboratory
Department of Chemistry
Chemical Engineering Division
Technical University Berlin
10623 Berlin, Germany

J. Peng, W. Hua
Institute for Applied Materials (IAM)
Karlsruhe Institute of Technology
Hermann-von-Helmholtz-Platz 1, 76344 Eggenstein-Leopoldshafen,
Germany

B. Wu, Z. Sofer
Department of Inorganic Chemistry
University of Chemistry and Technology Prague
Technická 5, Prague 6 166 28, Czech Republic

conditions,^[6] which are not conducive to the commercial desalination. Therefore, the development of novel types of 2D materials for photothermal conversion and solar desalination is a major challenge.

In recent years, metal-phosphorus-chalcogen (MPCh_x) complexes, which have a long history dating back to the 19th century, have attracted increasing attention.^[7] However, a comprehensive study of MPCh_x at the atomic level still has not yet been achieved.^[8] The general formulas of the MPCh_x could be represented as MPCh (e.g., PdPS and PdPSe), MPCh₃ (e.g., NiPS₃ and CoPS₃), and MPCh₄ (e.g., BiPS₄ and GaPS₄).^[9] The broader distribution of MPCh_x compared to TMDs on the periodic table, along with their greater chemical diversity and structural complexity, results in a greater variety of physical and chemical properties, as well as greater potential for applications.^[10] The most widely studied group is based on metal phosphorous trichalcogenides (MPCh₃), which exhibit a layered structure in which both P₂ pairs and metal atoms are in octahedral coordination, and van der Waals forces facilitate layer stacking.^[11] MPCh₃ have a wide range of layered compounds and tunable bandgap (1.3–3.5 eV),^[12] offering potential for photothermal conversion and solar desalination. However, to the best of our knowledge, there are currently no reports on the use of MPCh_x, including MPCh₃, for solar desalination. This is due to the poor stability of MPCh₃ in water and oxygen environments, which makes it unsuitable for direct use as a light converter.^[13] Therefore, it is worthwhile to explore suitable MPCh₃ nanosheets and design strategies for photothermal conversion and solar desalination.

As the typical MPCh₃ material, NiPS₃ nanosheet dispersions in organic solvents such as isopropanol (IPA) have attracted widespread attention,^[14] and its small band gap (≈ 1.42 eV)^[15] offers potential for photothermal conversion. The deposition of additives on the surface of 2D materials is an effective method to enhance their stability.^[16] However, some additives, such as aqueous polyvinyl alcohol (PVA) solution, cannot be directly mixed with NiPS₃ nanosheets dispersed in IPA. Therefore, developing a universal strategy to apply NiPS₃ nanosheets for efficient photothermal and solar desalination with high stability and studying the related photothermal conversion mechanism is of great importance.

Herein, we have successfully developed a universal mixed solvent exfoliation surface deposition (MSESD) strategy to utilize NiPS₃ nanosheets for photothermal conversion and solar desalination. In this work, we not only use IPA-water as a mixed solvent to efficiently prepare NiPS₃ nanosheet dispersions and avoid PVA precipitation, but also mainly deposit PVA on the edge of the NiPS₃ nanosheets and bond it to the sponge to prepare a stable converter. In particular, the prepared NiPS₃/PVA converter shows the high performance of photothermal conversion and solar desalination with an evaporation rate of 1.48 kg m⁻² h⁻¹ and an average photothermal conversion efficiency (PTCE) of 93.5% under a light intensity of 1 kW m⁻², which present the NiPS₃-based converter prepared using the MSESD strategy exhibits excellent photothermal conversion in the field of 2D materials. To our knowledge, this is the first report of MPCh_x for photothermal water evaporation and solar desalination. The entire preparation process is environmentally friendly, and the as-prepared converter has good stability. The investigation using scanning transmission electron microscopy (STEM), femtosecond transient absorption spectroscopy (fs-TAS), and photoluminescence (PL) revealed the photothermal conversion mechanism and showed that the energy of absorbed photons in NiPS₃ nanosheets can be effectively converted into heat through non-radiative photon transitions with phonons, defects or dangling surface bonds as well as multiple optical interactions, which promotes the enhancement of PTCE in the NiPS₃/PVA converter. This work provides new ideas and insights for the application of novel 2D materials in photothermal conversion and solar desalination.

2. Results and Discussion

The NiPS₃/PVA converter was prepared using the MSESD strategy as shown in Figure 1. First, the bulk NiPS₃ crystals were ground for 30 min using an agate mortar, with the continuous addition of IPA throughout the grinding process. As shown in Figure S1 (Supporting Information), the size of the NiPS₃ crystals effectively decreased under the action of shear force after the grinding. Inspired by the use of mixed solvents to adjust the surface tension to promote the exfoliation of MoS₂ nanosheets, the exfoliation of NiPS₃ was carried out using mixed solvents. The NiPS₃ crystals were sonicated in a mixed solvent of IPA and water in a volume ratio of 1:1 for mixed solvent exfoliation. The prepared 10 mL NiPS₃ nanosheet dispersions were then mixed with 1, 3, and 5 mL of 5 wt.% PVA aqueous solution, namely Ni10P1, Ni10P3, and Ni10P5, respectively. During this process, PVA was deposited on the surface of NiPS₃ nanosheets via surface deposition. Finally, 2 mL of the as-prepared Ni10P1, Ni10P3, and Ni10P5 solutions were evenly dropped on the blank sponge and dried at 110 °C to obtain Ni10P1-s, Ni10P3-s, and Ni10P5-s, respectively. Repeat several times until the dispersion is used up. It is worth noting that it is usually necessary to exfoliate the NiPS₃ nanosheets in IPA to efficiently prepare the stable NiPS₃/PVA nanocomposite dispersions. However, mixing the aqueous solution of PVA causes premature precipitation of the NiPS₃ nanosheets and PVA, which is not conducive to photothermal conversion and solar desalination (Figure S2a left and b, Supporting Information). Our MSEDE strategy cleverly solves this problem, and the prepared NiPS₃/PVA nanocomposite

J. Pezoldt
Fachgebiet Nanotechnologie
Institut für Mikro und Nanotechnologie
TU Ilmenau
Gustav-Kirchhoff-Str. 1, 98693 Ilmenau, Germany

A. Knauer
Institute of Micro- and Nanotechnologies MacroNano
TU Ilmenau
Gustav-Kirchhoff-Str.7, D-98693 Ilmenau, Germany

W. Hua
School of Chemical Engineering and Technology
Xi'an Jiaotong University
Xi'an, Shaanxi 710049, China

H. Wang, P. A. van Aken
Max Planck Institute for Solid State Research
Heisenbergstr. 1, 70569 Stuttgart, Germany
E-mail: hgwang@fkf.mpg.de

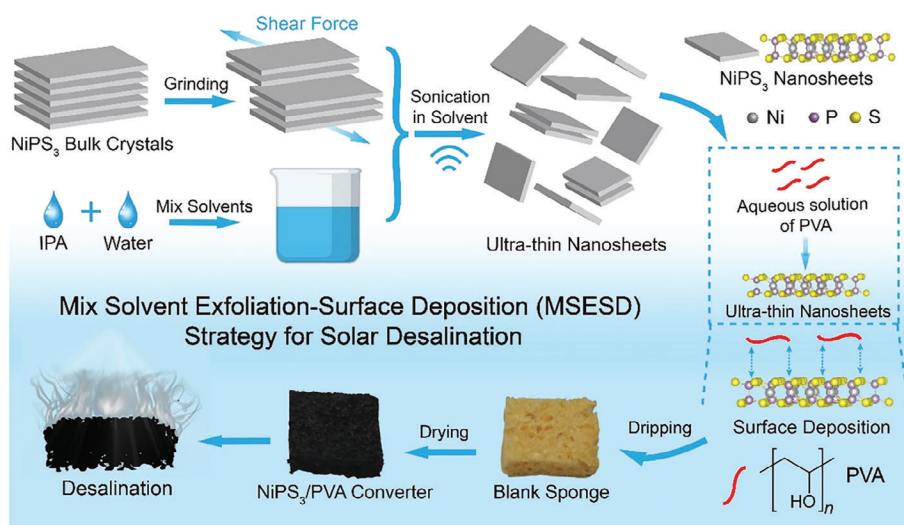


Figure 1. The preparation scheme of MSED strategy for solar desalination.

dispersions have good stability, providing a basis for efficient photothermal conversion and solar desalination (Figure S2a right, Supporting Information).

We then characterized the crystal structure and surface morphology of NiPS₃ nanosheets, Ni10P1, and Ni10P1-s using atomic force microscopy (AFM), scanning electron microscopy (SEM), and high-angle annular dark-field STEM (HAADF-STEM). The results in **Figure 2a–c** shows that we successfully fabricated few-layered ultrathin NiPS₃ nanosheets with a thickness of <3 nm (<4 layers).^[17] Compared with pure NiPS₃ nanosheets, the height of Ni10P1 is significantly increased to 13–21 nm (Figure 2b,c). This is because the PVA as a binder is deposited on the surface of the NiPS₃ nanosheets, causing the NiPS₃ nanosheets to be stacked. It also increases the number of internal reflections, refractions, and scattering of the incident light, which is beneficial for photothermal conversion.^[18] We further investigated the Ni10P1-s by SEM. Figure 2d shows that the pore diameters of the sponge are <50 μm and the water absorbed by the sponge would rise along the holes and accelerate desalination.^[19] Figure 2e shows that there are a large number of folds on the surface of the sponge, and Figure 2f suggests that a substantial amount of the prepared NiPS₃/PVA nanocomposites were successfully covered on the surface of the sponge, which is necessary for photothermal conversion and solar desalination. The large-scale HAADF-STEM image of Ni10P1 shows the distribution of NiPS₃ nanosheets (Figure 2g), which indicates the lateral size of the nanosheets, which is consistent with the AFM results (≈100 nm). In addition, HAADF-STEM results suggest that the prepared nanosheets have a crystal structure consistent with previous reports (Figure 2h).^[14] We also observed that the prepared nanosheets have point defects (Figure 2i), which is conducive to improving the photothermal conversion.^[20] Figure 2j shows the results of STEM electron energy-loss spectroscopy (EELS) maps, which reveal the presence of Ni, P, S, and C in Ni10P1, providing direct evidence for the successful preparation of the NiPS₃/PVA nanocomposites. In particular, C is mainly distributed at the edges of the NiPS₃ nanosheets. Since the edges

of MPCh₃ nanosheets are more susceptible to oxidation,^[13] the deposited PVA will effectively improve the stability of the NiPS₃ nanosheets, thereby promoting their stability in photothermal water evaporation.

X-ray absorption near-edge structure (XANES) and extended X-ray absorption fine structure (EXAFS) measurements were then performed to elucidate the electronic configuration and local environments of the NiPS₃ nanosheets. The white line position of the NiPS₃ nanosheets was nearly identical to that of the reference NiO from K-edge XANES (**Figure 3a**), indicating a +2 valence of Ni in the NiPS₃ nanosheets. In the corresponding Ni K-edge EXAFS spectra in the R-space of NiPS₃ (Figure 3b), a significant peak is observed at ≈2 Å, indicating the prominent presence of the Ni–S interatomic interaction.^[21] The crystal structures of NiPS₃ were then studied by X-ray diffraction (XRD) in the 2θ range from 10° to 80°. In Figure 3c, the peaks of bulk NiPS₃ are identified as monoclinic NiPS₃ (space group C2/m) (PDF No.78-0499).^[22] The NiPS₃ nanosheets show lower intensities and increased peak width, indicating that ultrathin 2D structures have been prepared.^[23] Figure 3d shows Raman spectra of NiPS₃ nanosheets and bulk NiPS₃ with an excitation laser line of 532 nm. Raman peaks from 50 to 600 cm⁻¹ originate from A_{1g} and E_g vibrational modes of the P₂S₆ units. The A_{1g} vibrational mode Raman peaks of NiPS₃ nanosheets showed a slight shift (≈2 cm⁻¹) due to the exfoliation of bulk NiPS₃ crystals, demonstrating the successful exfoliation of NiPS₃ nanosheets from the layered bulk NiPS₃ crystals.^[24] In Figure 3e, the UV–vis absorption spectra of NiPS₃ nanosheets and Ni10P1 almost completely overlap, indicating that PVA does not affect light absorption and photothermal conversion. Fourier-transform infrared (FTIR) spectra of NiPS₃ nanosheets, PVA, and Ni10P1 in the region of 250–4000 cm⁻¹ are shown in Figure 3f and Table S1. Bands at 270, 285, and 574.8 cm⁻¹ appeared in the FTIR spectrum, which is attributed to NiPS₃.^[25] For the Ni10P1, the typical bands at 856.4, 1411.9, 2939.0, and 3375.4 are attributed to C–C stretching, O–H/C–H bending, CH₂ asymmetric stretching, and O–H stretching, respectively, which also shows that we have successfully prepared NiPS₃/PVA nanocomposites.^[26] X-ray

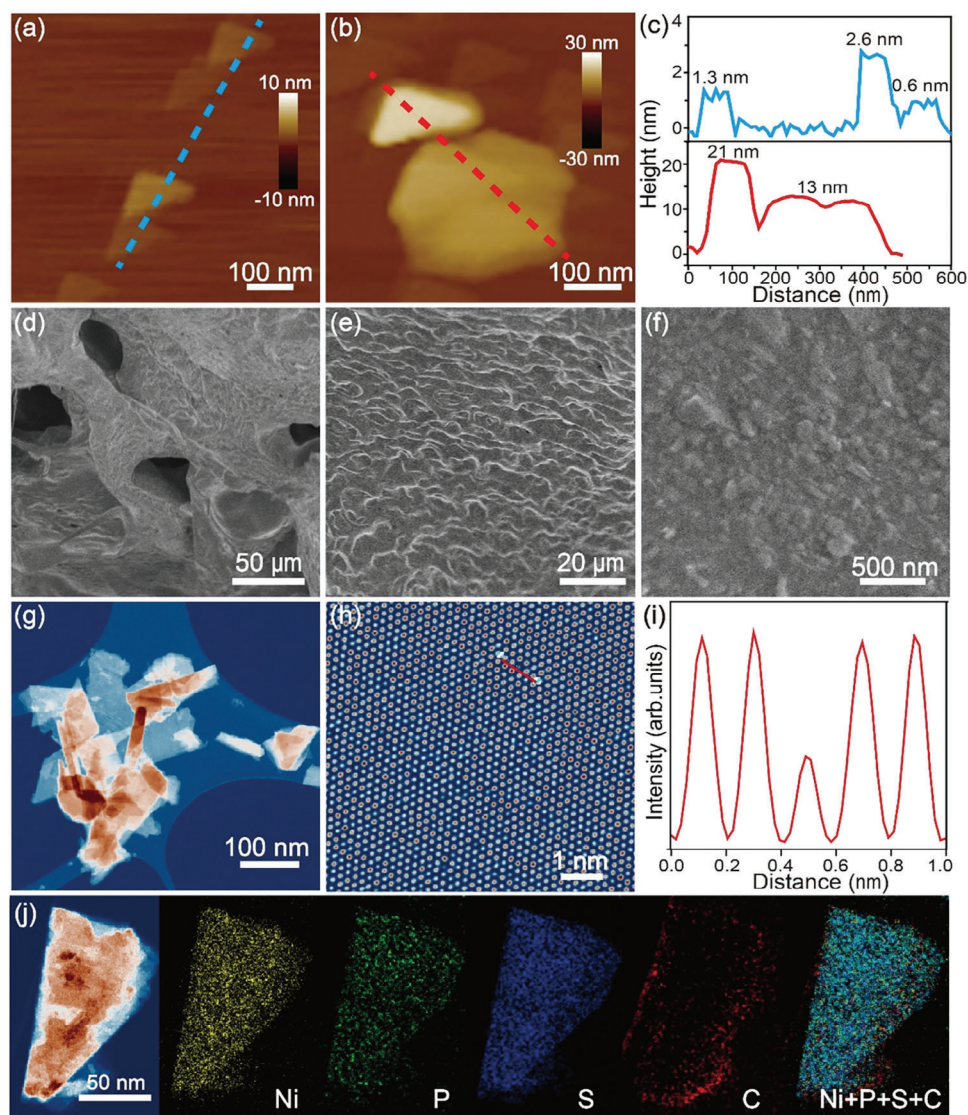


Figure 2. AFM images of exfoliated a) NiPS_3 nanosheets, b) Ni_{10}P_1 , and the corresponding height profiles c) top (NiPS_3 nanosheets) and bottom (Ni_{10}P_1). d–f) SEM images of Ni_{10}P_1 -s with increasing magnification. g) HAADF-STEM image and h) atomically resolved HAADF-STEM image of Ni_{10}P_1 i) with the HAADF intensity profile. j) HAADF-STEM image and the corresponding STEM-EELS maps of the Ni (yellow), P (green), S (blue), C (red), and their composite map, respectively.

photoelectron spectroscopy (XPS) was performed to measure the composition of NiPS_3 nanosheets. The characteristic Ni, P, S, C, and Si peaks are observed in Figure S3a (Supporting Information). High-resolution XPS spectra of NiPS_3 nanosheets (Figure S3b–d, Supporting Information) show peaks located at Ni 2p, P 2p, and S 2p, further suggesting that the exfoliated nanosheets are NiPS_3 .^[27]

We then investigated the optical and thermal properties and performance of Ni_{10}P_1 -s as a representative converter. Figure 4a shows the photograph of the blank sponge and Ni_{10}P_1 -s, indicating a size of $2 \times 2 \times 0.5 \text{ cm}^3$ for the converter. The sponge changed from yellow to black after the addition of Ni_{10}P_1 . Figure S4 (Supporting Information) shows that the blank sponge is a micrometer-scale porous structure, proving its high porosity, which is consistent with the SEM results. Figure 4b shows that

the converter is extremely light due to its low density and high porosity, and even a dandelion can withstand its weight without significant deformation, which is beneficial for subsequent water evaporation. To investigate the wettability of the Ni_{10}P_1 -s, we measured its contact angle before and after wetting, as shown in Figure 4c. The results show that, upon water drops on the Ni_{10}P_1 -s, it is quickly absorbed by the sample in less than one second, implying the Ni_{10}P_1 -s sample has excellent hydrophilic properties. This high hydrophilicity facilitates the easy penetration of water into the Ni_{10}P_1 -s and its movement to the surface through microchannels for solar-driven evaporation, where the superhydrophilic Ni_{10}P_1 -s converter can naturally float on water (Figure S5, Supporting Information).

Ni_{10}P_1 , Ni_{10}P_3 , and Ni_{10}P_5 were dripped onto a blank sponge to prepare the black Ni_{10}P_1 -s, Ni_{10}P_3 -s, and Ni_{10}P_5 -s

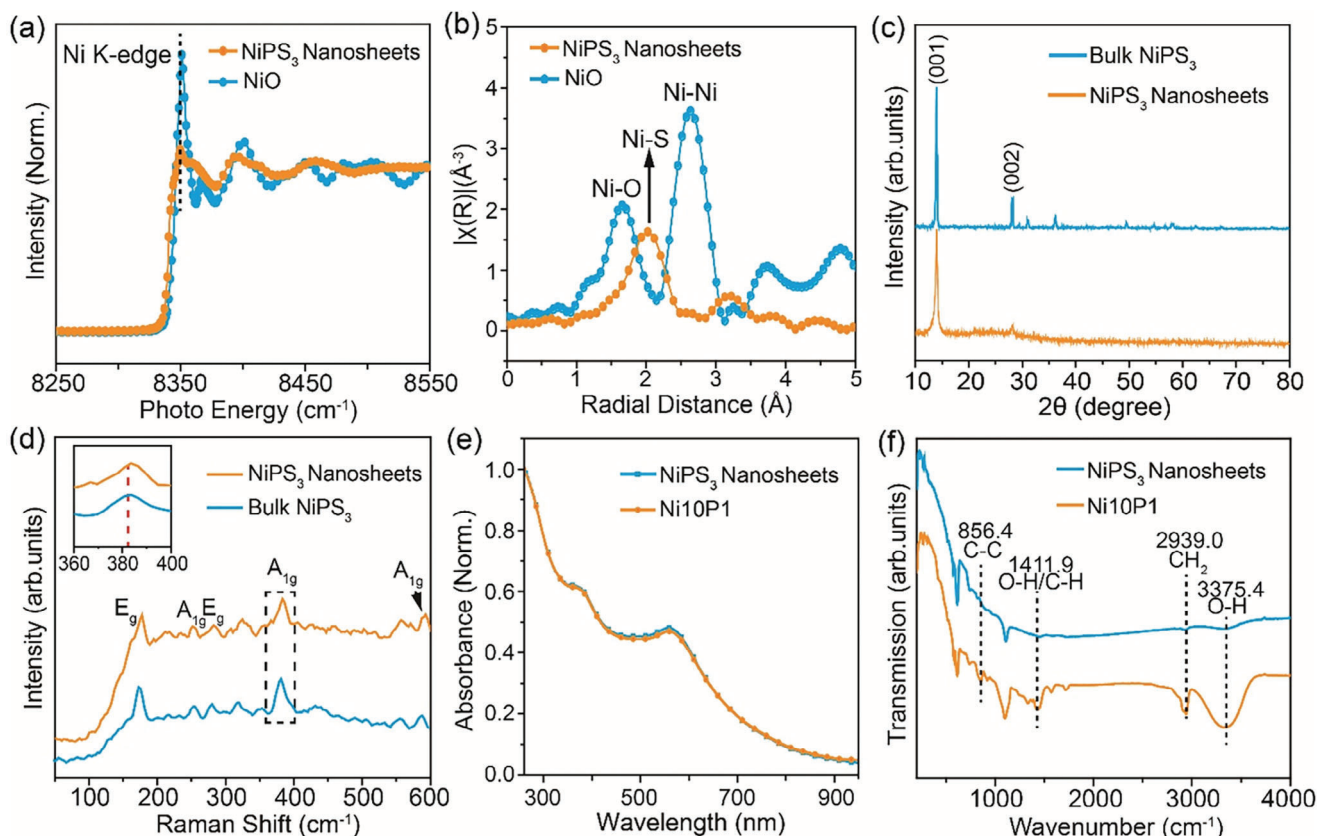


Figure 3. a) Normalized Ni K-edge XANES spectra of NiO and NiPS₃ nanosheets. b) The corresponding Ni K-edge R-space EXAFS spectra of NiO and NiPS₃ nanosheets. c) XRD patterns of bulk NiPS₃ and NiPS₃ nanosheets on the glass substrate. d) Raman spectra of bulk NiPS₃ and NiPS₃ nanosheets, and the corresponding enlarged Raman spectra (inset). e) Normalized UV-vis absorption spectra of NiPS₃ nanosheets and Ni10P1. f) FTIR spectra of NiPS₃ nanosheets and Ni10P1.

converters, which clearly show that Ni10P1-s has the lowest reflectance over a wide wavelength range from 250 to 2500 nm (Figure 4d), indicating that excessive addition of PVA cannot improve the PTCE of the NiPS₃-based solar converter. Furthermore, Figure 4e shows that the Ni10P1-s has a high absorption in the whole solar spectrum with an average absorption of $\approx 91.2\%$.^[28] This indicates that the converter has excellent light-harvesting capability and a strong ability to convert solar energy. Too high PVA content will hinder solar absorption and is not conducive to photothermal conversion. In a typical photothermal response experiment, we used Ni10Px samples to investigate the temperature change on the sample surface under an intensity of 1 kW m^{-2} (AM 1.5G). Figure 4f shows that the Ni10P1-s sample exhibits the fastest rising rate of increase in surface temperature upon illumination and gradually decreases to room temperature due to thermal equilibrium with the environment after the sunlight is removed. In particular, the surface temperature of Ni10P1 can reach 57°C within 300 s, demonstrating the best solar-to-thermal conversion performance. Meanwhile, Ni10P3-s and Ni10P5-s exhibit a rapid temperature rise process, with their surface temperatures reaching 56 and 54°C , respectively, after 300 s. This temperature rise is higher than the maximum temperature (30°C) reached by the blank sponge at the same time. The temperature difference ($\approx 27^\circ\text{C}$) indicates the excellent heat localization of

the NiPS₃-based converter, which is further confirmed by real-time infrared (IR) images (Figure 4g and Figure S6, Supporting Information). As shown in Figure S7 (Supporting Information), we conducted SEM tests on Ni10P3-s and Ni10P5-s. The results show that as the amount of PVA added increases, the sponge holes of Ni10P3-s (Figure S7a, Supporting Information) and Ni10P5-s (Figure S7b, Supporting Information) are significantly reduced or blocked compared with Ni10P1-s (Figure 2d), which will seriously limit their evaporation performance.

Then, the water evaporation and desalination performance of the NiPS₃/PVA converter was evaluated. To eliminate the interference of temperature and humidity,^[29] we conducted all the water evaporation experiments at $\approx 21^\circ\text{C}$ and $\approx 35\%$ RH. Figure 5a shows the schematic diagram of photothermal water evaporation, where the Ni10P1-s absorbs the solar energy and converts water into heat under solar light irradiation. The 3D porous structure of the sponge facilitates the transport of bulk water to the surface of the Ni10P1-s, which promotes the release of water vapor.^[30] Figure 5b shows IR images illustrating the rapid photothermal response and distinct equilibrium temperatures of the Ni10P1-s and a blank sponge when exposed to 1 kW m^{-2} of light. After 35 min, an equilibrium temperature difference of $\approx 7^\circ\text{C}$ is observed between the Ni10P1-s and the blank sponge. The corresponding surface temperature changes of the Ni10P1-s and the

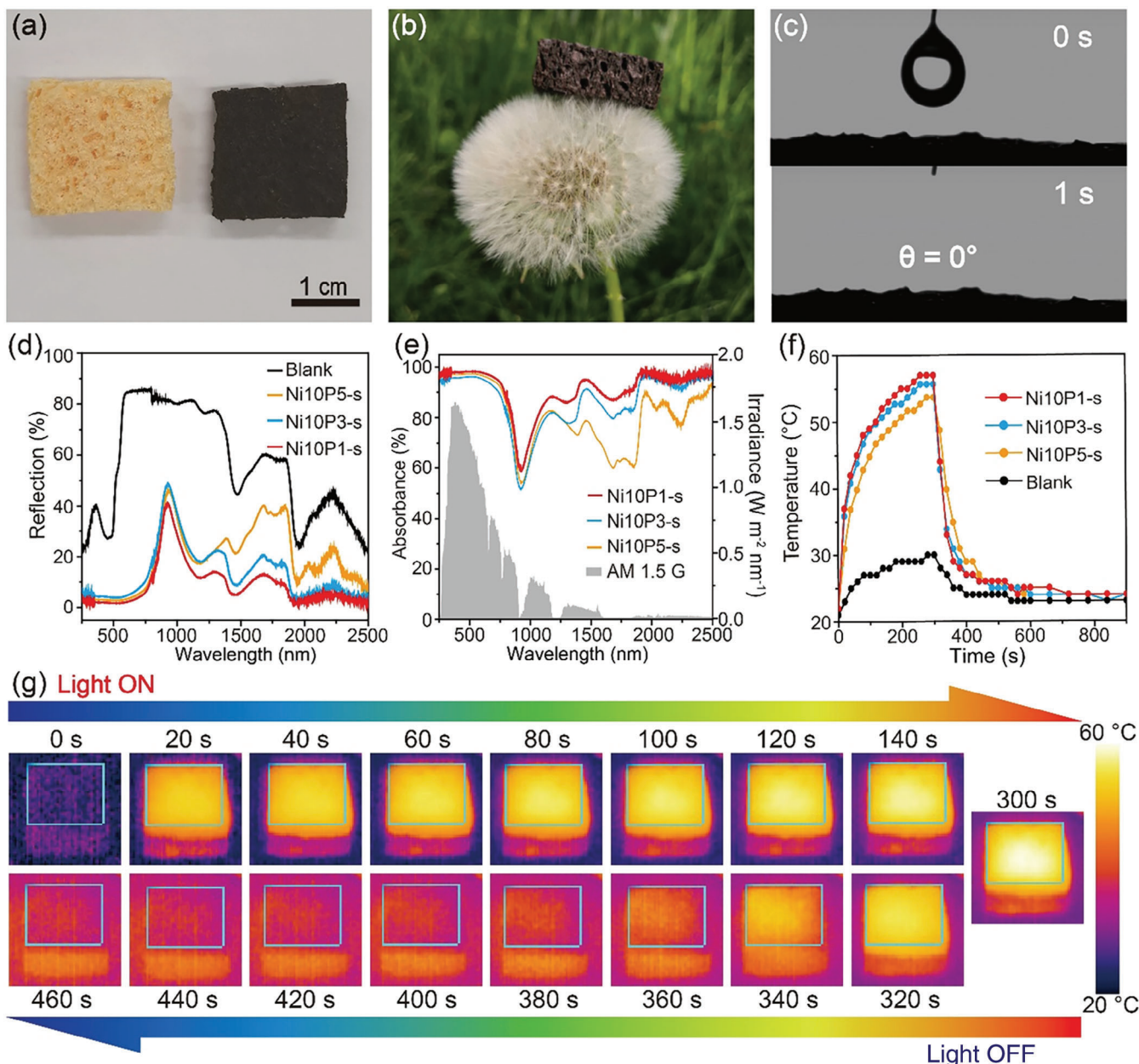


Figure 4. a) Photograph of the blank sponge (left) and Ni10P1-s (right). b) The photo shows the ultralight characteristics of the Ni10P1-s. c) Water contact angle measurements of Ni10P1-s. d) Reflection of the blank sponge, Ni10P1-s, Ni10P3-s, Ni10P5-s from wavelength 300 to 2500 nm. e) Absorbance of the Ni10P1-s, Ni10P3-s, and Ni10P5-s from wavelength 300 to 2500 nm. The inset is AM 1.5G solar spectrum. f) The surface temperature of blank sponge, Ni10P1-s, Ni10P3-s, Ni10P5-s changes with time when the Xe lamp is turned on or off under an optical density of 1 kW m^{-2} (1 sun). g) The real-time surface temperatures of Ni10P1-s are monitored by an IR camera under 1 sun irradiation for 300 s.

blank sponge are shown in Figure 5c. The surface temperature increases rapidly and stabilizes within 15 min. After 55 min, the temperatures of the Ni10P1-s in the stable state ($38 \text{ }^\circ\text{C}$) are higher than those of the blank sponge ($31 \text{ }^\circ\text{C}$) and the room temperature ($21 \text{ }^\circ\text{C}$), indicating a more efficient photothermal conversion of the Ni10P1-s.

The evaporation rate is evaluated by the mass loss of water, which is recorded with mass differences (Δm) at the beginning of evaporation ($t = 0 \text{ min}$) and at the end of evaporation

($t = 60 \text{ min}$) using an analytical balance. The following equation can be used:^[31]

$$r = \frac{\Delta m}{ST} \quad (1)$$

where r is the evaporation rate, Δm is the mass difference, S is the area of the light converter, and T is the evaporation time. The evaporation rates for pure water, empty sponge, and Ni10P1-s are

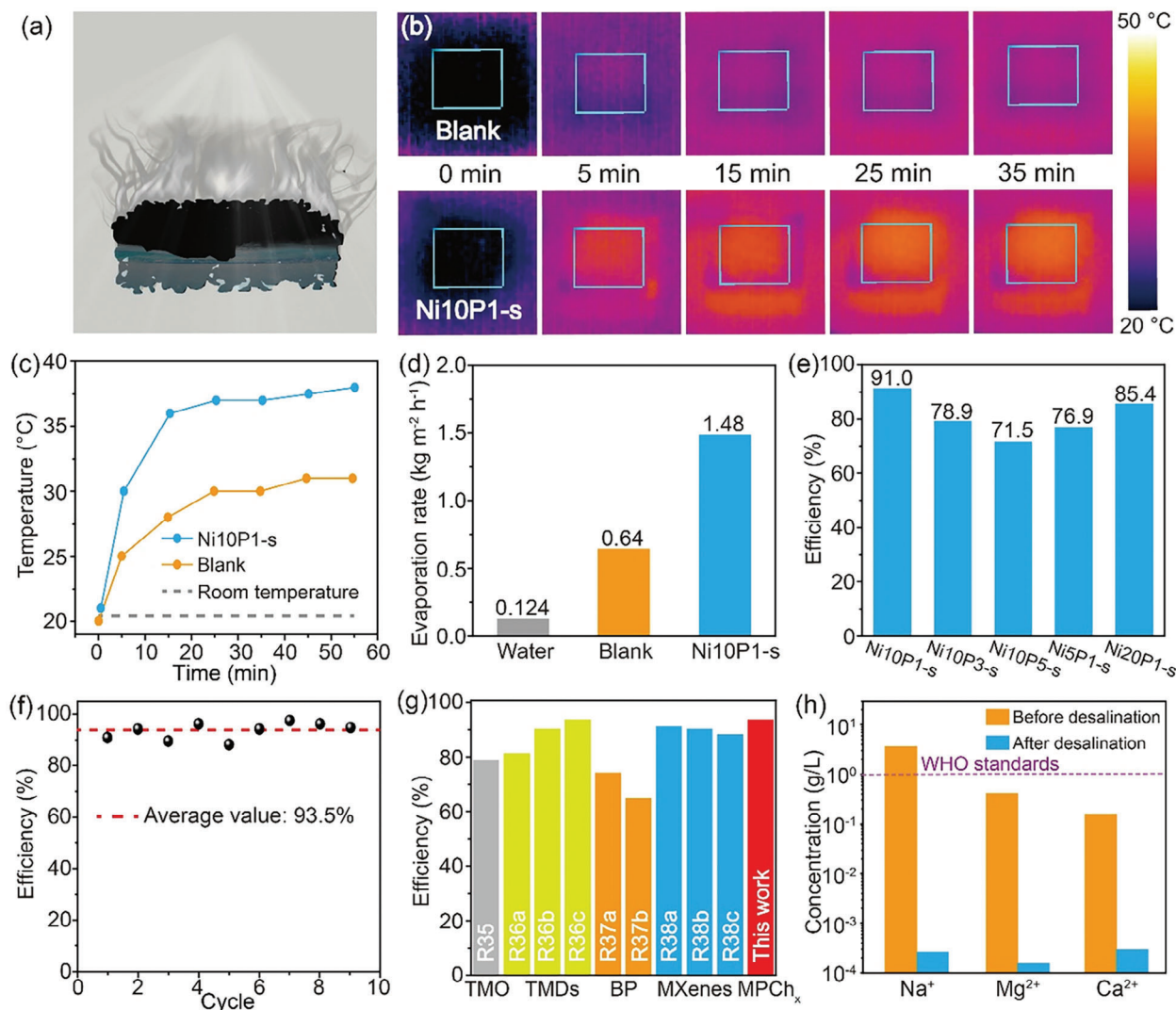


Figure 5. a) Schematic diagram of the experimental setup for photothermal water evaporation. b) Real-time surface temperatures of the blank sponge and Ni10P1-s are monitored by an IR camera under 1 sun irradiation for 35 min. c) Surface temperature change during photothermal water evaporation for the blank sponge and Ni10P1-s. d) Water evaporation results under different conditions. e) Photothermal conversion efficiencies for Ni10P1-s, Ni10P3-s, Ni10P5-s, Ni5P1-s, and Ni20P1-s. f) Cyclic water evaporation test of the Ni10P1-s. g) Comparison of the evaporation efficiency of this work with previously reported other 2D photothermal materials under 1 sun irradiation. h) The measured concentration of Na⁺, Mg²⁺, and Ca²⁺ before and after solar desalination.

shown in Figure 5d. Compared to pure water and blank sponge, the Ni10P1-s shows a more remarkable evaporation rate, providing 11.9 and 2.3 times improvement, respectively. In addition, we tested the mass changes of blank sponge and Ni10P1-s with time under 1 sun irradiation (Figure S8, Supporting Information). The mass changes in Ni10P1-s are larger than those in a blank sponge within 60 min. To investigate the impact of the size of 3D converters on the evaporation performance, the Ni10P1-s converter was prepared into square-shaped surfaces with side lengths of 2, 3, and 4 cm (Figure S9a, Supporting Information). The evaporation rate of different-sized evaporators decreased with an increase in the size of the evaporation surface (Figure S9b, Supporting Information). This changing trend is consistent with the previous report.^[32] We also changed the thickness of Ni10P1-s and blank sponge to 0.25, 0.5, and 1.0 cm and named them Sample-T-0.25,

Sample-T-0.5, and Sample-T-1.0 respectively, and then studied their evaporation rate under 1 sun irradiation (Figure S10, Supporting Information). The results show that the evaporation rate increases significantly when the thickness increases from 0.25 to 0.5 cm, while the change is not obvious when the thickness increases from 0.5 to 1.0 cm. This is attributed to the fact that, within certain limits, the thinner converter is not as efficient in localizing heat as the thicker ones, so some heat may be lost to the surroundings, causing the comparatively lower solar evaporation rate.

The evaporation rate can also be used to calculate the PTCE according to the following equation:^[33]

$$\eta = \frac{\Delta rh}{Q} \quad (2)$$

where η , Δr , h , and Q are the photothermal water evaporation efficiency, the evaporation rate difference (evaporation rate for the converter minus the evaporation rate for pure water in the dark), the evaporation enthalpy (2.43 kJ g^{-1}) of water at 303.15K, and the solar intensity, respectively. In addition, we obtained Ni5P1-s and Ni20P1-s by mixing 5 mL and 20 mL of NiPS₃ nanosheet dispersions with 1 mL of 5 wt.% PVA aqueous solution, respectively, and then dropping the resulting mixture onto a blank sponge and drying it at 110 °C. Compared with other converters, Ni10P1-s still has the highest PTCE, achieving a high PTCE of 91.0% under 1 sun irradiation (Figure 5e). The excellent photothermal water evaporation performance can be attributed to the excellent light trapping performance and unique hierarchical structure of the NiPS₃-based converter. In addition, Ni10P1-s exhibits superior stability for photothermal seawater evaporation, with an average PTCE of 93.5% over 9 cycles of the experiment (Figure 5f). This value is obviously higher than the average absorptance of Ni10P1-s of 91.2% because a hybrid hydrogel composed of a hydrophilic polymer framework (PVA) and absorber (NiPS₃) has internal capillary channels and the PVA can greatly promote the water evaporation owing to the reduced water evaporation enthalpy in the hydrogel network.^[34] It is worthwhile mentioning that the value of our NiPS₃-based converter is higher than the other 2D photothermal materials beyond graphene for photothermal water evaporation, such as transition metal oxides (TMOs),^[35] TMDs,^[36] BP,^[37] and MXenes,^[38] which perform the record evaporation rate under 1 sun irradiation (Figure 5g and Table S2). To evaluate the long-term stability and solid discharge of Ni10P1-s converter and the erosion behavior of NiPS₃ nanosheets during photothermal water evaporation, we conducted a 12 h photothermal water evaporation test under 1 sun irradiation. There was no obvious change in the appearance of the wet Ni10P1-s after the water evaporation (Figure S11a, Supporting Information), and no NiPS₃ material shedding off after removing wet Ni10P1-s was observed (Figure S11b, Supporting Information). In addition, we also used SEM to characterize the micromorphology of the Ni10P1-s after the water evaporation (Figure S12, Supporting Information). Compared with Figure 2d–f, the micromorphology of Ni10P1-s does not change significantly before and after the water evaporation, which shows that Ni10P1-s converter has good long-term stability and no obvious solid discharge and erosion behavior. When performing the photothermal water evaporation experiments, water will evaporate from the surface of the evaporator under solar light illumination, and subsequently water steam will condense on the thinner wall of the glass plate, then the desalinated water flows into a collection tube (Figure S13, Supporting Information). As evaporation proceeds, salt will gradually segregate on the surface of the converter (Figure S14, Supporting Information), which may be not beneficial for light absorption of the converter. However, removing the salt from the converter can continue to maintain evaporation performance. The results show that the NiPS₃-based converter prepared using the MSED strategy exhibits excellent photothermal conversion, which provides numerous opportunities for MPCh_x in photothermal conversion evaporation. In addition, Figure S15 (Supporting Information) shows that the peaks of XRD patterns remain almost unchanged before and after the 12 h water evaporation test. The peaks at $\approx 31^\circ$ and 45° are attributed to the formation of NaCl. The results further confirm the stabil-

ity of NiPS₃/PVA-based converters. We also investigated the effect of solar desalination in detail and found that three specific ions (Na⁺, Mg²⁺, and Ca²⁺) were significantly reduced, which was below the standards of the World Health Organization (WHO) (Figure 5h).^[39]

As discussed above, the NiPS₃ nanosheets have excellent light absorption in the UV–vis–NIR region to capture solar energy under irradiation. Non-thermal and/or radiative transition processes should be minimized to achieve better photothermal performance. To understand the light energy conversion process in NiPS₃ nanosheets, we measured the excited state dynamics of NiPS₃ in IPA/water using femtosecond transient absorption (fs-TAS) upon 387 nm photoexcitation (Figure 6a). The differential absorption spectra are shown in Figure 6b with time delays up to 7900 ps. Immediately after the excitation, ground state bleaching (GSB) with a minimum at 570 nm, which is well matched to the absorption seen in the steady-state absorption spectrum (Figure 3e), is accompanied by two broad positive excited state absorptions (ESAs) at 440–480 nm and 700–1400 nm. During the first 2 ps, these features are subject to blue shifts, indicating the cooling of hot excitons and/or the formation of multiexcitons. In particular, the rapid 2 ps decay of GSB is observed with an amplitude of $\approx 60\%$. Considering the non-emissive nature of NiPS₃ (Figure S16, Supporting Information), the fast exciton decay must be governed by non-radiative recombination. Thus, the energy of absorbed photons is likely to be transferred into the vibrations, namely a temperature increase of NiPS₃ nanosheets. A global analysis based on three sequential species is suitable to fit the fs-TAS data (Figure 6c,d). The three species have lifetimes of 1.81 ps, 187.08 ps, and 2.98 ns, respectively. The hot exciton is generated immediately after photoexcitation and is characterized by two dominant ESAs in the range of 440–480 nm and 700–1400 nm, together with a GSB centered at 570 nm. After 1.80 ps, the second species exhibits not only the same GSB and 440–480 nm ESA signatures as the first species, but also a blue-shifted 700–1400 nm ESA. We ascribe the second species with its 187.08 ps lifetime, to a mixture of cooled excitons and/or multiexcitons due to high-energy excitation. The third species, which shows the same characteristics as the second species, exists for 2.98 ns. Likely scenarios are that the relaxed excitons diffuse through different layers of NiPS₃ or are trapped at defect states. However, there is no emission during this time. This suggests a thermal transition. Moreover, all excitons decay within 2.98 ns, suggesting that the total thermal energy accumulation occurs on the same time scale. Most importantly, by comparing the differential optical density of GSB between the first and the third species, we conclude that $\approx 90\%$ of the excitons have decayed and that most of the thermal energy accumulation occurs in the region of 187.07 ps. Due to the low thermal diffusivity of pure PVA, the thermal energy dissipation of NiPS₃ after irradiation must be slower than the thermal accumulation, which rationalizes the high photothermal conversion efficiency.

Based on the experiments, we can use the following mechanism to explain the high PTCE of the NiPS₃-based converter: When a photon is absorbed, it can excite an electron to move from a low-energy ground state to a higher energy level. As shown in Figure S17 (Supporting Information), light with a photon energy higher than the band gap of the material can be absorbed

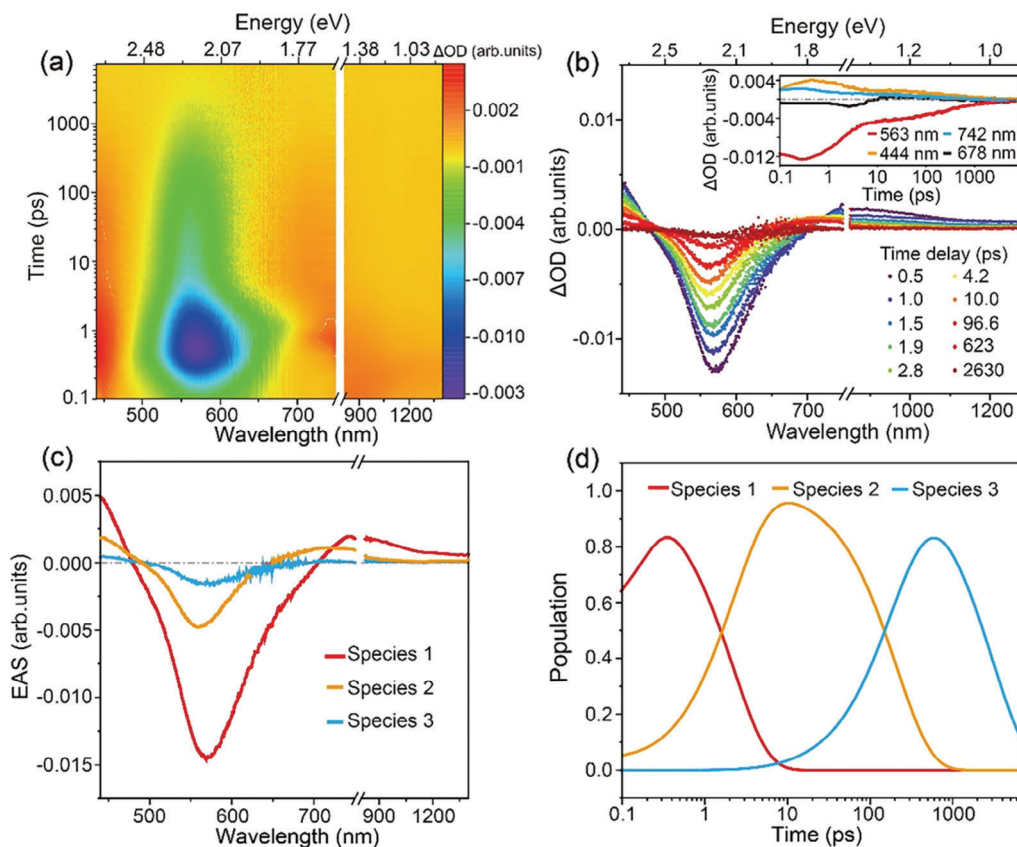


Figure 6. a) Heat map of fs-TAS raw data obtained from pump-probe experiments after photoexcitation at 387 nm with time delays up to 7900 ps. b) Differential absorption spectra at different time delays (ΔOD : differential optical density). Inset: Time absorption profiles and corresponding fits of selected wavelengths (see the figure legend for details). c) Evolution-associated spectra (EAS) of the deconvoluted species. d) Relative populations of each species with colors correlating with the EAS.

in semiconductors, causing electrons to move from the valence band (VB) to the conduction band (CB). These excited electrons are then relaxed to the bottom of the CB by a non-radiative relaxation process. The excited electron at the bottom of CB can be further recombined with a hole in the defect state by electron-phonon coupling through non-radiative recombination.^[40] Based on the HAADF-STEM, fs-TAS, and PL measurements, the radiative recombination is negligible, and thus the absorbed photon energy is mainly released by non-radiative phonons interacting with defects or surface dangling bonds. It is worth pointing out that although defects are beneficial to the photothermal effect, due to the low concentration of defects, may have limited help in improving the performance of photothermal water evaporation. On the other hand, photon energy smaller than the band gap of NiSP₃ can also be efficiently utilized by multiple interactions (Figure S18, Supporting Information), including multiple reflections, refractions, and scatterings.^[41] The multiple interactions with the NiPS₃ nanostructure are able to absorb infrared light by extending the effective length of light propagation, thus benefiting the PTCE. In this principle, the incident photons are more effectively trapped within the nanostructures, resulting in minimal photon leakage. As a result, the nanostructures can absorb the photon energy covering the entire solar spectrum and ultimately convert it into heat for water evaporation.

3. Conclusion

In summary, NiPS₃ nanosheets prepared from layered NiPS₃ bulk crystals were successfully applied to photothermal conversion and solar desalination based on the MSED strategy. In this strategy, we not only efficiently prepare the NiPS₃ nanosheet dispersions using IPA-water as the mixed solvent, but also mainly deposit PVA on the edge of NiPS₃ nanosheets to prepare a NiPS₃/PVA converter. The whole preparation process is environmentally friendly, and the prepared converter has good stability. The prepared converter shows high performance with an evaporation rate of 1.48 kg m⁻² h⁻¹ and an average PTCE of 93.5% under 1 sun irradiation. To our knowledge, this is the first report of MPCh_x for photothermal water evaporation and solar desalination. According to the relevant measurements, the first MPCh_x-based photothermal conversion mechanism is proposed, revealing that the energy of absorbed photons is efficiently transferred into the molecular vibrations as well as multiple optical interactions to satisfy the energy conversion. This work provides a facile and universal strategy for applying MPCh_x to photothermal conversion and solar desalination and provides important insights into the performance development of MPCh_x-based and 2D-based photothermal conversion materials.

Supporting Information

Supporting Information is available from the Wiley Online Library or from the author.

Acknowledgements

The Center of Micro- and Nanotechnology (ZMN), a DFG-funded core facility at TU Ilmenau, is gratefully acknowledged for professional support. H.W., Y.B., and P.C. were supported by the China Scholarship Council (CSC) scholarship. Z.S. was supported by the ERC-CZ program (project LL2101) from the Ministry of Education Youth and Sports (MEYS). B.W. was supported by the OP RDE registration no.: CZ.02.2.69/0.0/0.0/19_073/0016928, funded by the ESF. This work was partially funded through the European Union's Horizon 2020 research and innovation program under grant agreement No. 823717-ESTEEM3.

Open access funding enabled and organized by Projekt DEAL.

Conflict of Interest

The authors declare no conflict of interest.

Data Availability Statement

The data that support the findings of this study are available from the corresponding author upon reasonable request.

Keywords

2D materials, desalination, NiPS₃ nanosheets, photothermal conversions, surface depositions

Received: September 12, 2023
Revised: October 18, 2023
Published online:

- [1] a) P. Srimuk, X. Su, J. Yoon, D. Aurbach, V. Presser, *Nat. Rev. Mater.* **2020**, *5*, 517; b) Y. Zhang, Y. Wang, B. Yu, K. Yin, Z. Zhang, *Adv. Mater.* **2022**, *34*, 2200108; c) C. Lei, W. Guan, Y. Guo, W. Shi, Y. Wang, K. P. Johnston, G. Yu, *Angew. Chem., Int. Ed.* **2022**, *61*, e202208487.
- [2] a) H. Lu, W. Shi, Y. Guo, W. Guan, C. Lei, G. Yu, *Adv. Mater.* **2022**, *34*, 2110079; b) B. Yu, Y. Zhang, Y. Wang, Z. Zhang, *Adv. Funct. Mater.* **2023**, 2307533; c) H. Yu, D. Wang, H. Jin, P. Wu, X. Wu, D. Chu, Y. Lu, X. Yang, H. Xu, *Adv. Funct. Mater.* **2023**, *33*, 2214828.
- [3] a) L. Du, T. Hasan, A. Castellanos-Gomez, G. B. Liu, Y. Yao, C. N. Lau, Z. Sun, *Nat. Rev. Phys.* **2021**, *3*, 193; b) H. Kaur, J. N. Coleman, *Adv. Mater.* **2022**, *34*, 2202164; c) H. Wang, J. Shi, J. Zhang, Z. Tao, H. Wang, Q. Yang, P. A. Van Aken, R. Chen, *Nanoscale* **2022**, *14*, 12129.
- [4] a) X. Zhang, Z. Lai, C. Tan, H. Zhang, *Angew. Chem., Int. Ed.* **2016**, *55*, 8816; b) H. Wang, J. Niu, J. Shi, W. Lv, H. Wang, P. A. Van Aken, Z. Zhang, R. Chen, W. Huang, *Small* **2021**, *17*, 2102263.
- [5] a) Y. Wang, T. Guo, Z. Tian, K. Bibi, Y.-Z. Zhang, H. N. Alshareef, *Adv. Mater.* **2022**, *34*, 2108560; b) Y. Tang, C. Yang, X. Xu, Y. Kang, J. Henzie, W. Que, Y. Yamauchi, *Adv. Energy Mater.* **2022**, *12*, 2103867.
- [6] a) N. R. Glavin, R. Rao, V. Varshney, E. Bianco, A. Apte, A. Roy, E. Ringe, P. M. Ajayan, *Adv. Mater.* **2020**, *32*, 1904302; b) D. Yuan, Y. Dou, Z. Wu, Y. Tian, K. H. Ye, Z. Lin, S. X. Dou, S. Zhang, *Chem. Rev.* **2022**, *122*, 957.
- [7] M. Zhu, H. Kou, K. Wang, H. Wu, D. Ding, G. Zhou, S. Ding, *Mater. Horiz.* **2020**, *7*, 3131.
- [8] K.-Z. Du, X. Z. Wang, Y. Liu, P. Hu, M. I. B. Utama, C. K. Gan, Q. Xiong, C. Kloc, *ACS Nano* **2016**, *10*, 1738.
- [9] R. Gusmão, Z. Sofer, M. Pumera, *Angew. Chem., Int. Ed.* **2019**, *58*, 9326.
- [10] R. Brec, *Solid State Ion* **1986**, *22*, 3.
- [11] R. Samal, G. Sanyal, B. Chakraborty, C. S. Rout, *J. Mater. Chem. A* **2021**, *9*, 2560.
- [12] M. Barua, M. M. Ayyub, P. Vishnoi, K. Pramoda, C. N. R. Rao, *J. Mater. Chem. A* **2019**, *7*, 22500.
- [13] a) K. Synnatschke, J. Van Dinter, A. Müller, D. Tiede, L. Spillecke, S. Shao, D. Kelly, J. Konecny, B. Konkena, M. Mccrystal, N. Saigal, U. Wurstbauer, W. Bensch, Z. Sofer, J. N. Coleman, R. Klingeler, S. J. Haigh, C. Backes, *2D Mater.* **2023**, *10*, 024003; b) K. Synnatschke, S. Shao, J. Van Dinter, Y. J. Hofstetter, D. J. Kelly, S. Grieger, S. J. Haigh, Y. Vaynzof, W. Bensch, C. Backes, *Chem. Mater.* **2019**, *31*, 9127.
- [14] H. Wang, Y. Jiao, B. Wu, D. Wang, Y. Hu, F. Liang, C. Shen, A. Knauer, D. Ren, H. Wang, P. A. Van Aken, H. Zhang, Z. Sofer, M. Grätzel, P. Schaaf, *Angew. Chem., Int. Ed.* **2023**, *135*, e202217253.
- [15] J. Ran, H. Zhang, S. Fu, M. Jaroniec, J. Shan, B. Xia, Y. Qu, J. Qu, S. Chen, L. Song, J. M. Cairney, L. Jing, S. Z. Qiao, *Nat. Commun.* **2022**, *13*, 4600.
- [16] H. Ni, X. Liu, Q. Cheng, *J. Mater. Chem. A* **2018**, *6*, 7142.
- [17] S. Xue, L. Chen, Z. Liu, H. M. Cheng, W. Ren, *ACS Nano* **2018**, *12*, 5297.
- [18] F. Zhao, Y. Guo, X. Zhou, W. Shi, G. Yu, *Nat. Rev. Mater.* **2020**, *5*, 388.
- [19] Q. Wang, F. Jia, A. Huang, Y. Qin, S. Song, Y. Li, M. A. C. Arroyo, *Desalination* **2020**, *481*, 114359.
- [20] I. Ibrahim, D. H. Seo, A. M. McDonagh, H. K. Shon, L. Tijing, *Desalination* **2021**, *500*, 114853.
- [21] Y. Liu, Y. Chen, Y. Tian, T. Sakthivel, H. Liu, S. Guo, H. Zeng, Z. Dai, *Adv. Mater.* **2022**, *34*, 2203615.
- [22] R. Dangol, Z. Dai, A. Chaturvedi, Y. Zheng, Y. Zhang, K. N. Dinh, B. Li, Y. Zong, Q. Yan, *Nanoscale* **2018**, *10*, 4890.
- [23] H. Wang, W. Lv, J. Shi, H. Wang, D. Wang, L. Jin, J. Chao, P. A. Van Aken, R. Chen, W. Huang, *ACS Sustainable Chem. Eng.* **2020**, *8*, 84.
- [24] F. M. Oliveira, J. Pastika, V. Mazánek, M. Melle-Franco, Z. Sofer, R. Gusmão, *ACS Appl. Mater. Interfaces* **2021**, *13*, 23638.
- [25] C. Sourisseau, J. P. Forgerit, Y. Mathey, *J. Solid State Chem.* **1983**, *49*, 134.
- [26] a) A. Al-Hakimi, G. Asnag, F. Alminderej, I. Alhagri, S. Al-Hazmy, T. Qahtan, *Crystals* **2023**, *13*, 135; b) G. M. Kim, P. Simon, J. S. Kim, *Bioinspir. Biomim.* **2008**, *3*, 046003.
- [27] N. M. Latiff, C. C. Mayorga-Martinez, B. Khezri, K. Szokolova, Z. Sofer, A. C. Fisher, M. Pumera, *FlatChem* **2018**, *12*, <https://doi.org/10.1016/j.flatc.2018.11.003>.
- [28] Q. Gan, Y. Xiao, C. Li, H. Peng, T. Zhang, M. Ye, *Chemosphere* **2021**, *280*, 130618.
- [29] T. Gao, X. Wu, Y. Wang, G. Owens, H. Xu, *Sol. RRL* **2021**, *5*, 2100053.
- [30] P. Anukunwithaya, J. J. Koh, J. C. Chuan Yeo, S. Liu, X. Hou, N. Liu, C. He, *J. Mater. Chem. A* **2022**, *10*, 15743.
- [31] J. Wang, Y. Li, L. Deng, N. Wei, Y. Weng, S. Dong, D. Qi, J. Qiu, X. Chen, T. Wu, *Adv. Mater.* **2017**, *29*, 1603730.
- [32] T. Gao, Y. Wang, X. Wu, P. Wu, X. Yang, Q. Li, Z. Zhang, D. Zhang, G. Owens, H. Xu, *Sci. Bull.* **2022**, *67*, 1572.
- [33] P. Cheng, H. Wang, H. Wang, P. A. Van Aken, D. Wang, P. Schaaf, *Adv. Energy. Sust. Res.* **2021**, *2*, 2000083.
- [34] X. Zhou, F. Zhao, Y. Guo, Y. Zhang, G. Yu, *Energy Environ. Sci.* **2018**, *11*, 1985.
- [35] X. Ming, A. Guo, G. Wang, X. Wang, *Sol. Energ. Mater. Sol. C.* **2018**, *185*, 333.
- [36] a) X. Yang, Y. Yang, L. Fu, M. Zou, Z. Li, A. Cao, Q. Yuan, *Adv. Funct. Mater.* **2018**, *28*, 1704505; b) J. Xiao, Y. Guo, W. Luo, D. Wang, S. Zhong, Y. Yue, C. Han, R. Lv, J. Feng, J. Wang, W. Huang, X. Tian, W. Xiao, Y. Shen, *Nano Energy* **2021**, *87*, 106213; c) P. Liu, Y.-B. Hu, X. Y.

- Li, L. Xu, C. Chen, B. Yuan, M. L. Fu, *Angew. Chem., Int. Ed.* **2022**, *61*, 202208587.
- [37] a) M. Li, Q. Zhao, S. Zhang, D. Li, H. Li, X. Zhang, B. Xing, *Environ. Sci. Nano* **2020**, *7*, 414; b) Z. Li, W. Cai, X. Wang, Y. Hu, Z. Gui, *J. Colloid Interf. Sci.* **2021**, *582*, 496.
- [38] a) Y. Lu, D. Fan, Y. Wang, H. Xu, C. Lu, X. Yang, *ACS Nano* **2021**, *15*, 10366; b) K. Li, T. H. Chang, Z. Li, H. Yang, F. Fu, T. Li, J. S. Ho, P.-Y. Chen, *Adv. Energy Mater.* **2019**, *9*, 1901687; c) H. Zhang, X. Shen, E. Kim, M. Wang, J. H. Lee, H. Chen, G. Zhang, J. K. Kim, *Adv. Funct. Mater.* **2022**, *32*, 2111794.
- [39] P. Cheng, M. Ziegler, V. Ripka, H. Wang, K. Pollok, F. Langenhorst, D. Wang, P. Schaaf, *ACS Appl. Mater. Interfaces* **2022**, *14*, 16894.
- [40] K. Wang, Y. Hou, B. Poudel, D. Yang, Y. Jiang, M. G. Kang, K. Wang, C. Wu, S. Priya, *Adv. Energy Mater.* **2019**, *9*, 1901753.
- [41] P. Cheng, D. Wang, P. Schaaf, *Adv. Sustain. Syst.* **2022**, *6*, 2200115.